


## Article

# Experimental Investigation of the Thermal Runaway Propagation Characteristics and Thermal Failure Prediction Parameters of Six-Cell Lithium-Ion Battery Modules

Hongxu Li <sup>1</sup>, Qing Gao <sup>1,2</sup> and Yan Wang <sup>3,4,\*</sup> <sup>1</sup> College of Automotive Engineering, Jilin University, Changchun 130025, China; ooaxus@163.com (H.L.)<sup>2</sup> State Key Laboratory of Automotive Simulation and Control, Jilin University, Changchun 130025, China<sup>3</sup> School of Mechanical and Automotive Engineering, Qingdao University of Technology, Qingdao 266525, China<sup>4</sup> State Key Laboratory of Automotive Safety and Energy, Tsinghua University, Beijing 100084, China

\* Correspondence: wangyan2387@163.com

**Abstract:** Efforts to meet regulations ensuring the safety of lithium-ion battery (LIB) modules in electric vehicles are currently limited in their ability to provide sufficient safe escape times in the event of thermal runaway (TR). Thermal runaway occurs when the heat generation of a battery module exceeds its heat removal capacity, leading to a rapid increase in temperature and uncontrolled heat release. To address this issue, this study focuses on evaluating the cascading thermal failure characteristics of six-cell LIB modules under an air environment in an experimental combustion chamber. Sensors are strategically placed at advantageous locations to capture changes in various characteristic parameters, including LIB temperature, module voltage, module mass, and the concentrations of venting gases in the combustion chamber. Analysis of the variations in these characteristic parameters over time aims to identify effective signals that can predict thermal failure conditions with a maximum warning time. The results demonstrate that monitoring LIB temperature provides the shortest advance warning of TR propagation within the module. However, module voltage measurements offer a warning that is approximately 2% earlier on average. On the other hand, measurements of the module mass and concentrations of venting gases in the combustion chamber allow for warnings of thermal failure that are, on average, approximately 2 min earlier than those based solely on LIB temperature. These findings can serve as guidance for improving the safety of LIBs, enhancing the reliability of fault detection systems, and exceeding the safe escape time requirements set by current global regulations.

**Keywords:** lithium-ion battery module; thermal runaway propagation; failure characteristics; fire warning; combustion



**Citation:** Li, H.; Gao, Q.; Wang, Y. Experimental Investigation of the Thermal Runaway Propagation Characteristics and Thermal Failure Prediction Parameters of Six-Cell Lithium-Ion Battery Modules. *Energies* **2023**, *16*, 5172. <https://doi.org/10.3390/en16135172>

Academic Editor: Antonino S. Arico

Received: 26 May 2023

Revised: 25 June 2023

Accepted: 30 June 2023

Published: 5 July 2023



**Copyright:** © 2023 by the authors. Licensee MDPI, Basel, Switzerland. This article is an open access article distributed under the terms and conditions of the Creative Commons Attribution (CC BY) license (<https://creativecommons.org/licenses/by/4.0/>).

## 1. Introduction

The increasing market share of electric vehicles has led to the development of numerous safety regulations concerning lithium-ion battery (LIB) technologies used as power sources. Among these regulations, those focusing on fire safety are particularly critical. The most significant concern in terms of fire safety is thermal runaway (TR), which occurs when a battery module generates more heat than it can dissipate, resulting in a rapid temperature rise and uncontrolled heat release. For instance, the United Nations' Global Technical Regulation No. 20 on electric vehicle safety mandates a minimum of five minutes of advance warning against hazardous conditions caused by TR. Meeting such regulations necessitates the accurate identification of critical failure parameters during the early stages of TR and a comprehensive understanding of TR propagation characteristics within LIB modules.

Currently, numerous studies are dedicated to addressing these crucial issues related to the fire safety of LIB modules. For instance, Börger et al. [1] analyzed the TR properties

of LIB modules from a fundamental scientific perspective, aiming to facilitate standardized analysis of TR phenomena. Other studies have investigated the factors contributing to TR, influential elements, suppression methods, and prediction models for LIB module TR [2]. Notably, analyses of precipitating and influencing factors have elucidated the roles played by various aspects of TR phenomena, such as the initial status of LIBs, including their state of charge (SOC) and state of health (SOH) [3–5], environmental conditions like initial pressures and temperatures [6], material factors [7,8], triggering conditions [9,10], triggering modes and scales [11,12], battery types [13,14], battery arrangement [15,16], and the degree of battery aging [17]. Suppression methods have been proposed based on the development of internal components and external interventions, such as phase change materials [18], heat pipes [19], and two-phase sprays [20]. Additionally, theoretical modeling has been employed to predict TR phenomena in LIB modules [4].

Several studies have conducted experimental investigations into thermal runaway (TR) phenomena in single-battery lithium-ion battery (LIB) modules. For instance, Wang et al. [21] evaluated the impact of battery aging on TR processes by experimentally comparing fresh and aged cells under external heating. The results demonstrated that aged cells exhibited a higher TR onset temperature and lower reactivity, resulting in a reduced rate of temperature increase, higher flame temperature, and decreased mass loss compared to fresh cells. In contrast to externally triggered TR conditions, Hao et al. [22] experimentally studied the effect of state of charge (SOC) on the mechanical properties and failure mechanisms of single-battery LIB modules under bending loads. The results revealed that the flexural modulus and stiffness of the battery increased with SOC, and failure mechanisms such as delamination, interlayer slippage, and electrode cracking were observed. Zhao et al. [23] employed novel experimental equipment to assess the influence of environmental conditions on TR behavior in single-battery LIB modules, considering both enclosed and ventilated conditions. The results highlighted that external pressure played a crucial role in case rupture, with a greater risk of gas explosion observed in enclosed conditions compared to ventilated conditions.

Ostaneck et al. [24] developed a coupled model to simulate heat and gas generation in LIB modules during TR onset and evolution. The results provided estimations of time-to-venting and time-to-TR values, offering practical guidance for the design of safer batteries. While the aforementioned studies have provided valuable insights for the design of safe LIBs, the behavior of a single-battery LIB module cannot fully represent the TR propagation characteristics within a multiple-battery module pack. TR propagation in these modules occurs through a combination of thermal resistance networks among modules and the influencing factors of TR [25,26]. Several studies have addressed this issue. For example, Feng et al. [27] experimentally characterized TR propagation triggered by nail penetration of the first battery in an LIB module comprising six cells. The study found that fire had little influence on TR propagation but caused significant damage to battery accessories. Heat transfer through the battery shell was identified as the dominant heat transfer process. Huang et al. [28] investigated the thermal properties and combustion characteristics of LIB modules containing seven cells arranged in rhombus and parallel layouts. Critical temperatures triggering TR propagation were obtained and validated using classical Semenov and Frank-Kamenetskii models. The methodology can be applied to explore other LIB configurations. Liu et al. [29] developed a numerical finite-element thermo-kinetic model to study TR properties in single LIBs using COMSOL Multiphysics software. The model was then applied to an LIB module comprising six cells, producing results that aligned well with experimental data. Other studies examined TR propagation characteristics in multiple-LIB modules resulting from gas venting due to the rupture of a Li-ion cell [30,31]. In addition to gas generation and jet flow, Mao et al. [32] investigated the dynamic combustion properties of a single 18650-type LIB using a lumped model. The Arrhenius equation and isentropic flow equations were utilized to simulate gas generation and venting processes, respectively, with results validated through comparisons with experimental data. Parameters such as internal battery pressure, gas ejection speeds,

flame shape, and height provided guidance to enhance LIB pack safety. Cai et al. [33] incorporated experimentally measured gas venting parameters, particularly the volume-averaged CO<sub>2</sub> concentration in the vent-channel, as an upper bound for the detection threshold to meet the 5-min safety warning required by Global Technical Regulation No. 20. The authors indicated that combining multiple sensor types could enhance the confidence of the detection system.

As evident from the aforementioned discussion, experimental methods have proven to be more intuitive and reliable than modeling approaches in characterizing the thermal runaway (TR) propagation and combustion properties of multiple lithium-ion battery (LIB) modules. However, previous efforts to meet and surpass minimum safe escape time regulations have been limited due to an incomplete understanding of the battery parameters that provide the earliest possible warning of TR conditions in multiple-LIB modules. This study addresses this limitation by conducting combustion tests based on the national testing standard GB/T20284-2006 [34], which applies to individual building materials and products. The tests aim to evaluate the cascading thermal failure characteristics of six-cell LIB modules in an air environment. The dynamic thermal properties of the system during induced TR propagation are captured using an infrared camera, and sensors are strategically placed to measure various characteristic parameters, including LIB temperature, module voltage, module mass, and the concentrations of venting gases in the combustion chamber. The variations in these parameters over time are analyzed to identify effective signals that can predict thermal failure conditions with the maximum warning time. This research provides valuable guidance for enhancing the safety of LIBs, improving the reliability of fault detection systems, and extending the safe escape time beyond the requirements of Global Technical Regulation No. 20.

## 2. Battery Modules

The six-cell LIB modules employed in this study are illustrated in Figure 1, and included commercial prismatic Li(Ni<sub>0.6</sub>Mn<sub>0.2</sub>Co<sub>0.2</sub>)O<sub>2</sub>/graphite LIBs, an aluminum-plastic stand, a busbar, an aluminum sheet, end plates on both sides, and upper and lower insulation plates. The individual LIBs employed in the modules had dimensions of 54 mm × 145 mm × 95 mm, charge-discharge capacities of 104 Ah, and nominal voltages of 3.75 V. The key parameters of the resulting LIB modules are listed in Table 1.

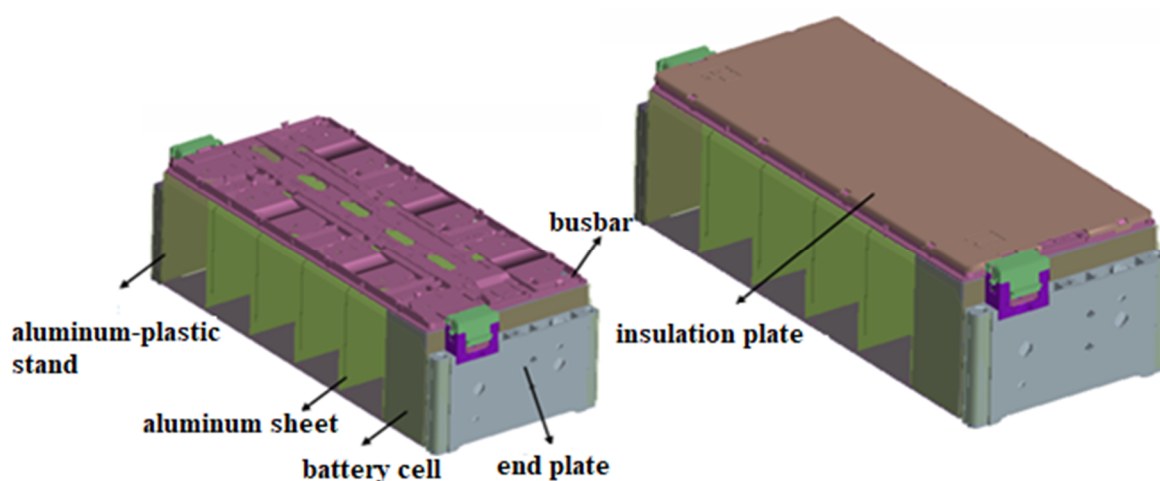
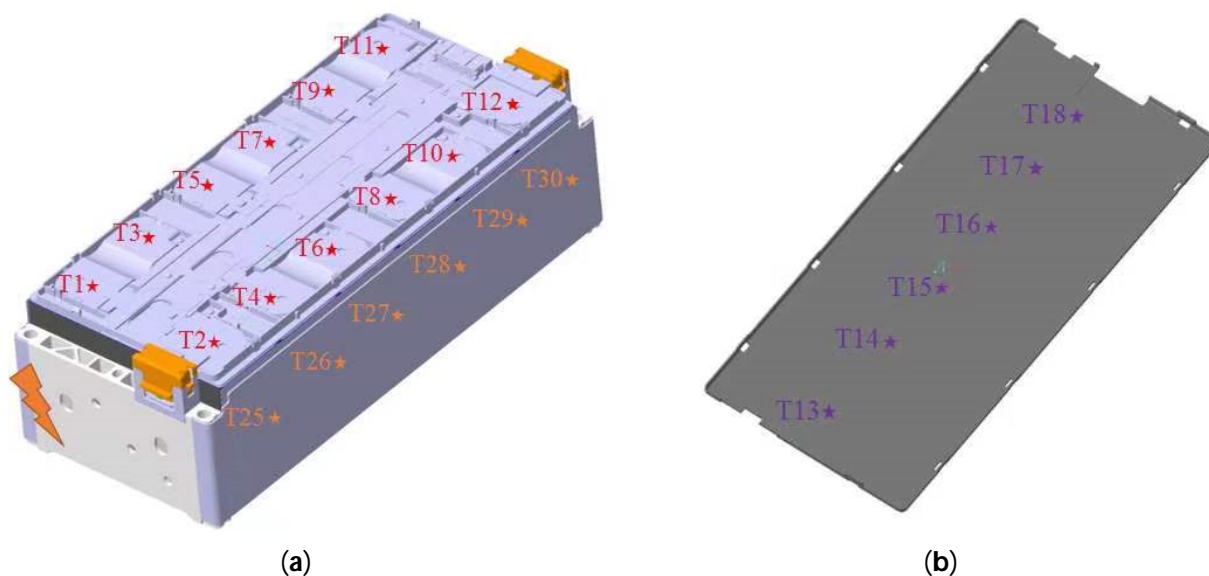


Figure 1. Illustration of the LIB modules employed in the experiments.

**Table 1.** Key parameters of the LIB modules employed in the experiments.

| Battery Architecture         | 6S1P            |
|------------------------------|-----------------|
| Nominal module capacity (Ah) | 104             |
| Nominal module voltage (V)   | 21.96           |
| Module mass (kg)             | 11.04           |
| Module dimensions (mm)       | 355 × 151 × 108 |

Prior to testing, all LIBs in the module were discharged to the cut-off voltage, and then charged to an SOC of 100% at a rate of 1/3C. As shown in Figure 2, the 30 numbered temperature measurement points were uniformly arranged on the positive and negative tabs of the busbar (temperature measurement points 1–12), the upper cover of the insulation plate (measurement points 13–18), and the center of the battery side wall (measurement points 19–24 and 25–30) to comprehensively detect the thermal field of the module. Finally, the charged module was placed in a constant temperature environment at 25 °C for 24 h to ensure that the charge state and temperature of the module were stable prior to testing.



**Figure 2.** Temperature measurement points of the experimental setup. (a) points 1–12 and 19–30. (b) points 13–18.

### 3. Experimental Setup

The experimental setup used to assess the thermal runaway (TR) propagation characteristics of the lithium-ion battery (LIB) modules is depicted in Figure 3. The test system primarily consists of a combustion chamber, a 400 W radiative heater, an array of vertical-gradient thermocouples to measure the center temperature of the fire plume, a smoke/gas vent system equipped with thermocouples, pressure sensors, and O<sub>2</sub> concentration sensors, and a gas analyzer for independent measurement of CO and CO<sub>2</sub> concentrations. The heater was positioned 30 cm away from LIB1 to initiate TR propagation. A data collector was incorporated into the system to capture real-time signals from thermocouples, voltage sensors, and an electronic scale, which provide information on the fire plume temperature, thermal field of the module, LIB voltages, and module mass, respectively. Additionally, an infrared camera recorded the real-time temperature distribution of the LIB module. The smoke/gas generated in the combustion chamber were expelled using an exhaust fan at the vent inlet, and the exhaust gas passed through a particle filter before entering the gas analyzer, which transmitted its data to a computer. The smoke/gas vent system also included an anemometer to detect the direction of gas flow in the vent tube. The

thermocouple array used to measure the fire plume temperature consisted of a bundle of 30 armored thermocouples spaced vertically at 10 cm intervals above the insulation plate of the LIB module, with a horizontal spacing of 5 cm.

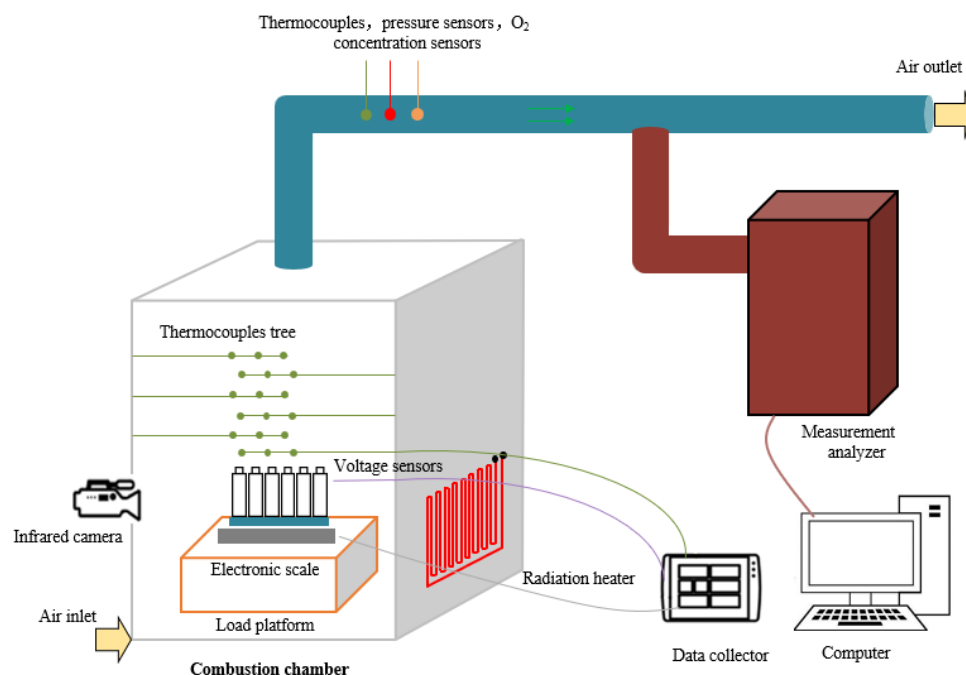


Figure 3. Experimental combustion setup.

#### 4. Experimental Process

Prior to testing, the initial mass of the LIB module was independently measured using an electronic scale. The module was then securely fixed in the center of the load platform of the combustion chamber, with an insulation pad placed in between to protect the scale from thermal damage. All equipment was powered up at the beginning of the testing process, ensuring proper ventilation by starting the exhaust fan. The heater was set to a constant power of 400 W to initiate the TR (thermal runaway) process. The timing of the heating process was initiated as soon as the heater was activated. Once the combustion process was completed, the heater was powered down. This experimental process was repeated three times independently, and the observed mass losses of the LIB modules were 3974 g, 3827 g, and 3679 g respectively. The low relative error of 3.4% indicates good consistency among the experimental results. All the results presented below are based on the data collected from a single six-cell module.

#### 5. Results and Discussion

##### *Thermal Runaway Propagation Behavior*

Representative infrared imagery shows the progression of thermal runaway (TR) as Figure 4, and the initial release of smoke/gas at 1526 s. The highest recorded flame temperature reached 134.1 °C. At 1540 s, a jet fire occurred, followed by the formation of a second jet flame at 1574 s. At 1580 s, two flames were observed, accompanied by flying sparks. The flame temperature then significantly decreased until 2121 s. A second smoke/gas release event occurred at 2371 s, demonstrating typical eddy and entrainment behavior. At 2372 s, two flames simultaneously formed and continued to burn stably until 2390 s, with subsequent temperature reduction until 2807 s. A third smoke/gas ejection event occurred at 2924 s, accompanied by three flames. At 2928 s, the smoke underwent deflagration, reaching a maximum temperature of 570 °C. The module entered a stable burning period at 2931 s, with a maximum temperature of 931.5 °C, followed by temperature reduction until 3466 s. The same sequence of smoke/gas ejections, flame



eruptions, stable combustion, and temperature decrease occurred twice more starting at 3475 s and 4064 s. Finally, the module entered a cooling stage, with the temperature decreasing to 333.3 °C at 7260 s.

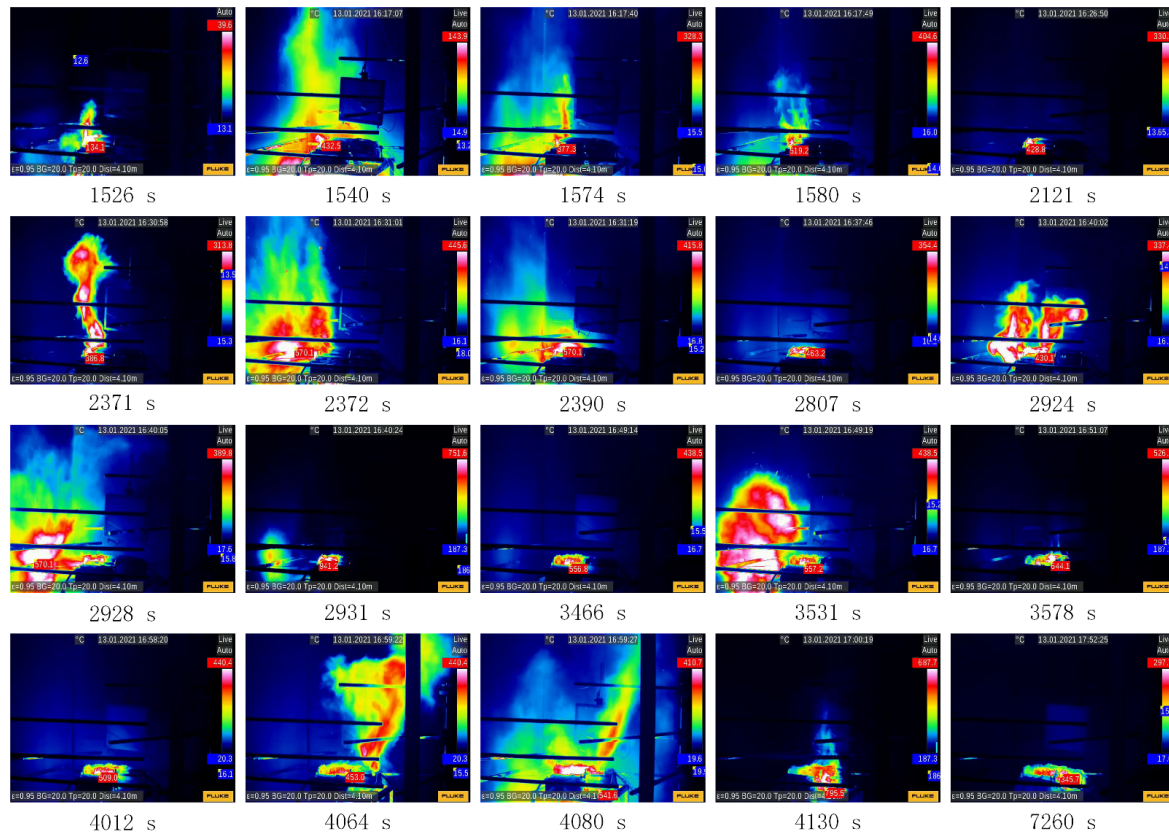


**Figure 4.** Infrared imagery indicative of TR propagation and combustion behaviors observed within an LIB module.

Based on the provided description, five smoke/gas ejection events occurred at 1526 s, 2371 s, 2924 s, 3475 s, and 4064 s. The thermal failure of the LIB cells led to the emission of high-speed jets of flammable smoke with significant turbulence. Collisions and reactions between the flammable smoke and oxygen molecules resulted in the formation of additional jet flames, while the high-temperature smoke diffused and spread into the open space of the combustion chamber. For example, the two observed jet flames at 2372 s demonstrated the formation of a vortex at the jet boundaries due to the large velocity difference between the high-speed jets and the surrounding environment. Additionally, the jets continuously drew in the surrounding air, supporting the observed combustion behavior. In contrast, the uneven fuel mixing in the third jet eruption at 2924 s was due to the relatively low turbulent kinetic energy of the jet gas, resulting in an increasing flame height. The fourth jet eruption at 3531 s exhibited a short flame, followed by deflagration after the fuel fully mixed with the air. Finally, in the fifth eruption at 4064 s, two cells erupted almost simultaneously, and the rapid jet flows caused the flame to rapidly ascend, separate, and extinguish.

## 6. Analysis of Characteristic Parameters of Failure

### Temperature Characteristics

The temperatures observed for each LIB in the module at the positive tabs of the busbar (temperature measurement points 1, 3, 5, 7, 9, and 11) during the TR process are respectively presented along with the peak temperature values in Figure 5 as a function of time. As can be seen, the temperatures of the six LIBs all manifested notable fluctuations consistent with the discussion of Figure 4 above.

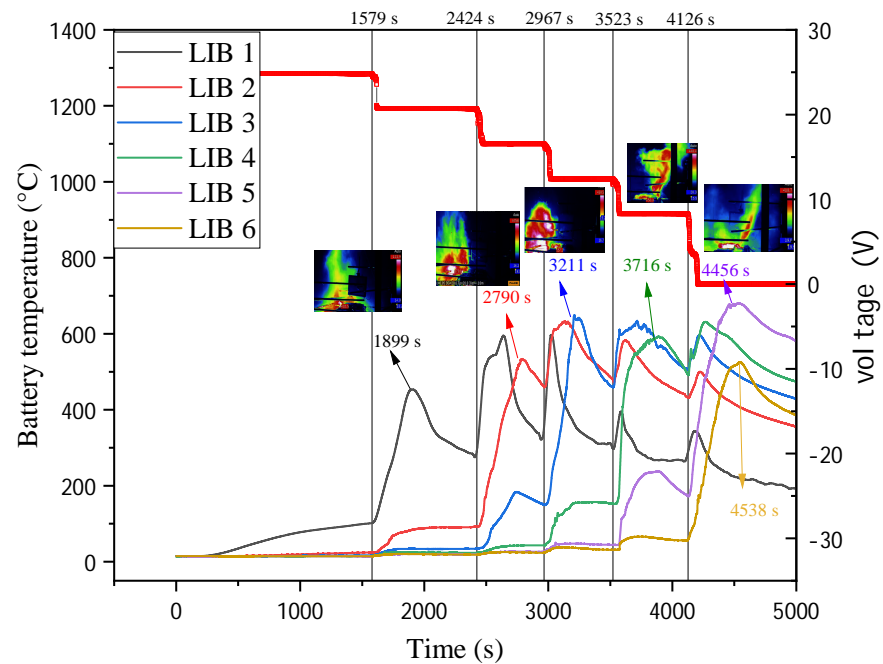


**Figure 5.** Temperature of each LIB observed at the positive tab of the busbar (temperature measurement points 13, 14, 15, 16, 17, and 18) during the TR process along with peak temperature values.

We can now analyze the TR propagation process in the experimental module based on the presented results. The first temperature peak was observed in LIB 1 battery at 1904 s, and heat transfer did not cause the failure of the other LIBs. For LIB 2 battery, the first temperature peak occurred at 2790 s, slightly later than the second peak observed in LIB 1. However, TR had already been initiated in LIB 1 at its first temperature peak, although the temperature of LIB 1 was significantly increased due to its proximity to the high temperature of LIB 2. At this stage, heat transfer was limited within the module. As heat propagated through the module, LIB 3 exhibited a temperature peak at 3211 s, slightly earlier than the third peak of LIB 1 battery and the second peak of LIB 2. The first temperature peak of LIB 4 appeared at 3716 s, slightly earlier than the fourth peak of LIB 1, the third peak of LIB 2, and the second peak of LIB 3. Similarly, the first peak of LIB 5 occurred at 4456 s, earlier than the fifth peak of LIB 1, the fourth peak of LIB 2, the third peak of LIB 3, and the second peak of LIB 4. Clearly, the high temperature of LIB 2 had a significant effect on the temperature levels of the subsequent LIBs. Finally, it is worth noting that the temperature peak of LIB 6 at 4538 s was slightly earlier than the second peak of LIB 5. However, by this point, LIBs 1–5 had already burned out due to the complete combustion of all combustible materials, so the temperature fields of LIBs 1–5 did not influence LIB 6.

We can also determine the initiation time of TR for each LIB by examining the derivative of temperature with respect to time ( $dT/dt$ ) for each LIB in the module, as shown in Figure 6. Using a threshold of  $dT/dt \geq 6$  as the criterion for TR initiation, indicated by the horizontal line in Figure 6, we can observe that TR was initiated in LIB 1 at 1591 s, in LIB 2 at 2453 s, in LIB 3 at 2966 s, and in LIBs 4, 5, and 6 at 3552 s, 4137 s, and 4139 s respectively. Based on these findings, we can determine that the time difference between the initiation of TR in LIBs 1 and 2 was 858 s, the time difference between LIBs 2 and 3 was 507 s, the time difference between LIBs 3 and 4 was 586 s, and the time difference between LIBs 4 and 5 was 585 s. Additionally, the time difference between the initiation of TR in LIBs 5 and 6 was only 2 s, indicating that TR was initiated almost simultaneously in these two LIBs.

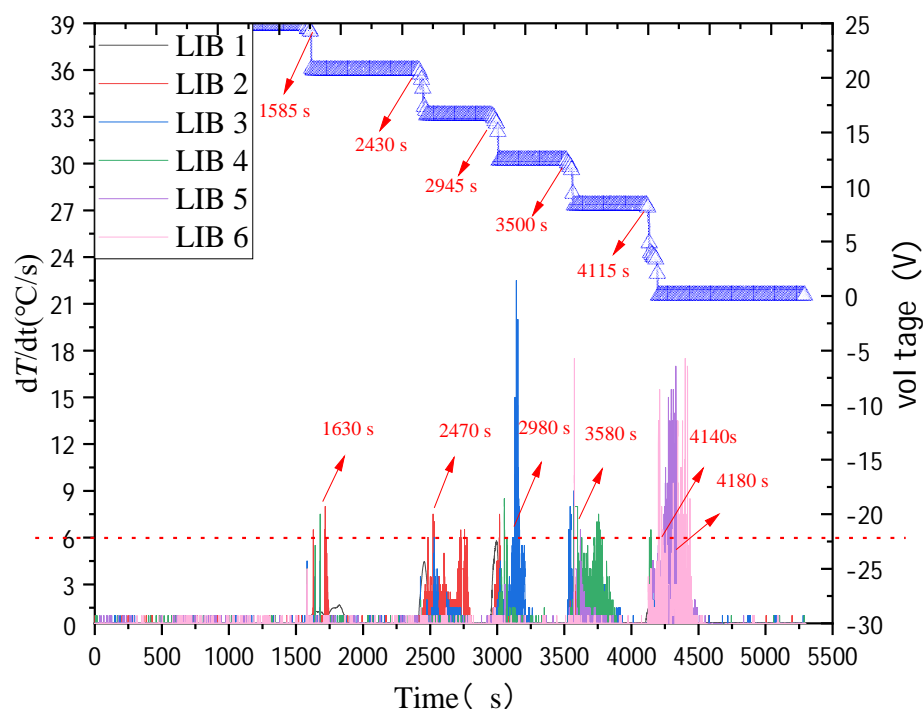


**Figure 6.** Derivatives of the LIB temperatures in Figure 5 with respect to time ( $dT/dt$ ) and Voltages of each LIB are plotted for comparison.

### 7. Voltage Characteristics

The total voltage of the six-cell LIB module is represented by the blue curve in Figure 6, plotted as a function of time during the TR process. It is evident that the total voltage shows a stepwise decrease, corresponding to the propagation of TR. The knee-point voltages of the LIB module were recorded as 24.8 V, 21.1 V, 16.9 V, 13.1 V, 8.5 V, and 0 V at 1585 s, 2430 s, 2945 s, 3500 s, 4115 s, and 4193 s respectively. Consequently, a five-stage voltage drop process occurred in decrements of 4.2 V, 4.2 V, 4.2 V, 4.2 V, and 8.3 V respectively.

By comparing the observed temporal voltage characteristics with the TR initiation times obtained for the six LIBs (1630 s, 2470 s, 2980 s, 3580 s, 4140 s, and 4180 s), we can conclude that the knee-point voltages were obtained 45 s, 40 s, 35 s, 80 s, 35 s, and 13 s in advance of the TR initiation times based on the temperature parameter. This represents a relative advance of +2%, or an average of 41 s. Therefore, using the voltage drop signal as a criterion provides a warning that occurs, on average, 41 s earlier than the temperature change rate of the module.

### 8. Mass Characteristics

The mass of the LIB module observed during the TR process is plotted as a function of time in Figure 7. It is evident that the mass of the module also shows a stepwise decrease, corresponding to the propagation of TR. The mass losses of 585 g, 600 g, 665 g, 621 g, and 1284 g occurred over five rapid declining steps from 1445 s to 1500 s, 2290 s to 2335 s, 2840 s to 2885 s, 3400 s to 3440 s, and 3985 s to 4040 s respectively. The durations of these five steps were 55 s, 55 s, 45 s, 40 s, and 55 s, and the corresponding mass loss rates were 10.64 g/s, 10.91 g/s, 14.78 g/s, 15.53 g/s, and 23.34 g/s respectively.

Some additional details regarding the mass loss results are of interest in this context. Firstly, the high mass loss rate of 23.34 g/s observed in the fifth stage occurred due to the almost simultaneous initiation of TR in LIBs 5 and 6. Furthermore, a fluctuation in the module weight was observed during the first stage, initially decreasing to 11,073 g at 1489 s before increasing to 11,679 g. This irregularity can be attributed to the perturbation in weight caused by the movement of the insulation cover under the force of gases escaping from LIB 1 during its failure. It is worth noting that the module mass remained relatively



constant between the rapidly decreasing mass events during the periods 1500–2290 s, 2335–2840 s, 2885–3400 s, and 3440–3985 s. This can be attributed to the damage to the upper insulation cover during the first flame eruption in stage 1, which created a direct connection between the inside of the module and the external environment. This weakened the impact of the smoke/gas generated during subsequent eruptions.

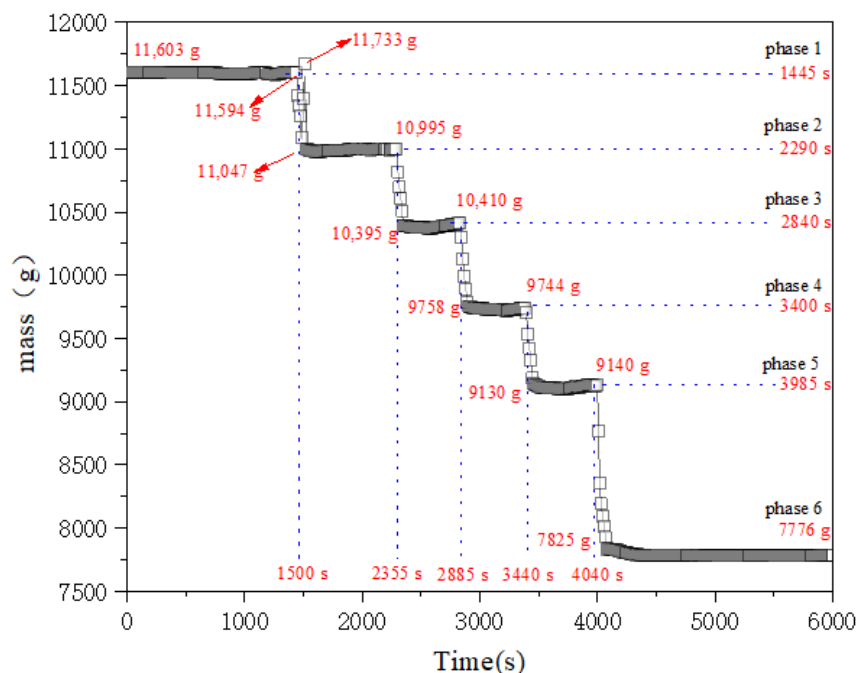
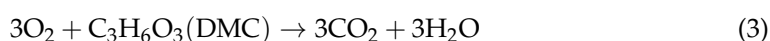
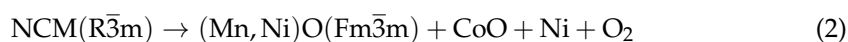
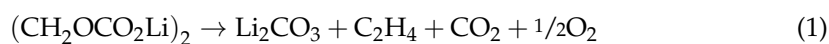


**Figure 7.** Mass of the module as a function of time during the TR process.

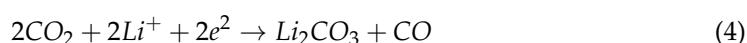
When compared to using the temperature change rate or voltage drop of the module, it becomes evident that the rapid reduction in module mass provides an earlier warning. Specifically, the temporal positions of the knee points of the module mass at 1445 s, 2290 s, 2840 s, 3400 s, and 3985 s are 146 s, 163 s, 126 s, 152 s, and 152 s earlier than those of the temperature parameter (i.e., 1591 s, 2453 s, 2966 s, 3552 s, and 4137 s).

## 9. Smoke/Gas Characteristics

High temperature conditions within an LIB initiate a series of overlapping and alternating decomposition reactions among the battery materials, which include solid electrolyte interphase (SEI) film decomposition, electrolyte decomposition, and electrode decomposition and reactions with the electrolyte. These reactions are given as follows [35].



Here, the lithium nickel cobalt manganese oxide (NCM) cathode decomposes according to Equation (2). At the same time, the  $\text{CO}_2$  produced by the above reactions reacts with  $\text{Li}^+$  ions to form lithium carbonate and CO as follows.



In addition, these reactions do not exclude the oxidative conversion of CO to CO<sub>2</sub> in open space.

The concentrations of O<sub>2</sub>, CO<sub>2</sub>, and CO by volume observed in the combustion chamber during the TR process are plotted in Figure 8 as a function of time. It is evident from the graph that the concentrations of these three reaction products were correlated at 1470 s, 2320 s, 2860 s, 3430 s, and 4010 s. Specifically, at these reaction events, the O<sub>2</sub> concentration exhibited minimum values of 19.1 vol%, 19.4 vol%, 19.4 vol%, 19.4 vol%, and 18.4 vol%, resulting in corresponding O<sub>2</sub> consumptions of 1.9 vol%, 1.6 vol%, 1.6 vol%, 1.6 vol%, and 2.6 vol%.

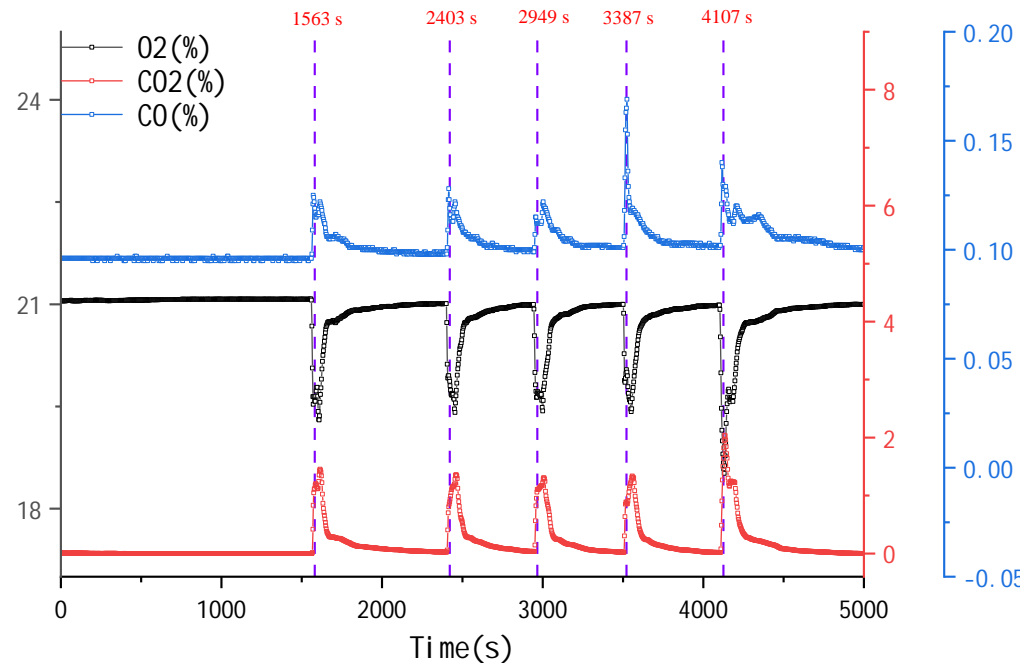


**Figure 8.** Measured O<sub>2</sub>, CO<sub>2</sub>, and CO concentrations by volume in the combustion chamber as a function of time during the TR process.

The gas produced by the oxidation reaction of smoke primarily consists of CO and CO<sub>2</sub>, which is reflected in the curves showing five peaks accordingly. While the background level of CO<sub>2</sub> was typically very low, it increased by 1.5 vol%, 1.4 vol%, 1.4 vol%, 1.4 vol%, and 2.1 vol% at these reaction events. In contrast, the background level of CO was generally high, with the CO concentration increasing by 0.13 vol%, 0.13 vol%, 0.13 vol%, 0.17 vol%, and 0.15 vol% at these reaction events. Therefore, the production of CO<sub>2</sub> by volume was generally greater than that of CO.

We further note that heat is released continuously while the flue smoke/gas reacts with oxygen in the combustion chamber. Therefore, the heat release rate (HRR) is a parameter characterizing the intensity of smoke combustion. Obviously, the associated fire hazard increases as the HRR increases.

The HRR can be calculated by the oxygen consumption method according to the following formula.

$$HRR = \left[ E\phi - (E_{CO} - E) \frac{1 - \phi X_{CO}}{2 X_{O_2}} \right] \frac{m_a}{1 + \phi(a - 1)} \frac{M_{O_2}}{M_a} (1 - X_{H_2O}) X_{O_2} \quad (5)$$

Here,  $E$  is the heat released per 1 kg of oxygen consumed by combustion (MJ/kg),  $E_{CO}$  is the heat released by CO consuming 1 kg of oxygen (17.6 MJ/kg),  $\phi$  is an oxygen consumption factor,  $X_{CO}$ ,  $X_{O_2}$ , and  $X_{H_2O}$  are the respective molar concentrations CO, O<sub>2</sub>, and H<sub>2</sub>O,  $m_a$  is the mass flow rate of gas before and after combustion,  $M_{O_2}$ , and  $M_a$  are the respective molar masses of O<sub>2</sub> and the air originally in the combustion chamber (kg/mole),

and  $a$  is an expansion factor, which is usually a value of 1.105. The factor  $\phi$  is required to correct for the difficulty of measuring  $m_a$  because the combustion tests of the failed module were conducted in an open space. This is addressed by defining  $\phi$  as follows:

$$\phi = \frac{X_{O_2}^0(1 - X_{CO_2} - X_{CO}) - X_{O_2}(1 - X_{CO_2}^0)}{(1 - X_{O_2} - X_{CO_2} - X_{CO})X_{O_2}^0}, \quad (6)$$

where  $X_{CO_2}$  is the molar concentration of  $CO_2$ , and  $X_{CO_2}^0$  and  $X_{CO_2}$  are the respective initial molar concentrations of  $O_2$  and  $CO_2$  measured before the combustion experiment. Finally, we define  $m_a$  as follows:

$$m_a = C \sqrt{\frac{\Delta P}{T_a}}, \quad (7)$$

where  $\Delta P$  is the pressure difference of gas passing through the pipe (Pa), and  $T_a$  is the temperature of the gas at the pipe (K).

The experimentally obtained gas concentration values presented in Figure 8 were used in Equations (5)–(7) to calculate the Heat Release Rate (HRR), and the resulting HRR values are plotted in Figure 9 as a function of time. It is evident from the graph that there are five distinct peaks in the HRR curve, corresponding to temporal points of 1470 s, 2320 s, 2860 s, 3430 s, and 4010 s as shown in Figure 8. These peaks have HRR values of 18.4 kW/m<sup>2</sup>, 18.7 kW/m<sup>2</sup>, 16.8 kW/m<sup>2</sup>, 13.7 kW/m<sup>2</sup>, and 27.3 kW/m<sup>2</sup>, respectively. Notably, the fifth gas jet resulted in the highest HRR peak value due to the simultaneous failure of LIBs 5 and 6, which generated a significant volume of smoke. The relatively lower HRR peak value of the fourth gas jet can be attributed to the significant increase in CO concentration by 0.17 vol% during that reaction event (Figure 8). This increase was caused by the high temperature peak observed in LIB 3 (Figure 6) following the third smoke/gas ejection event.

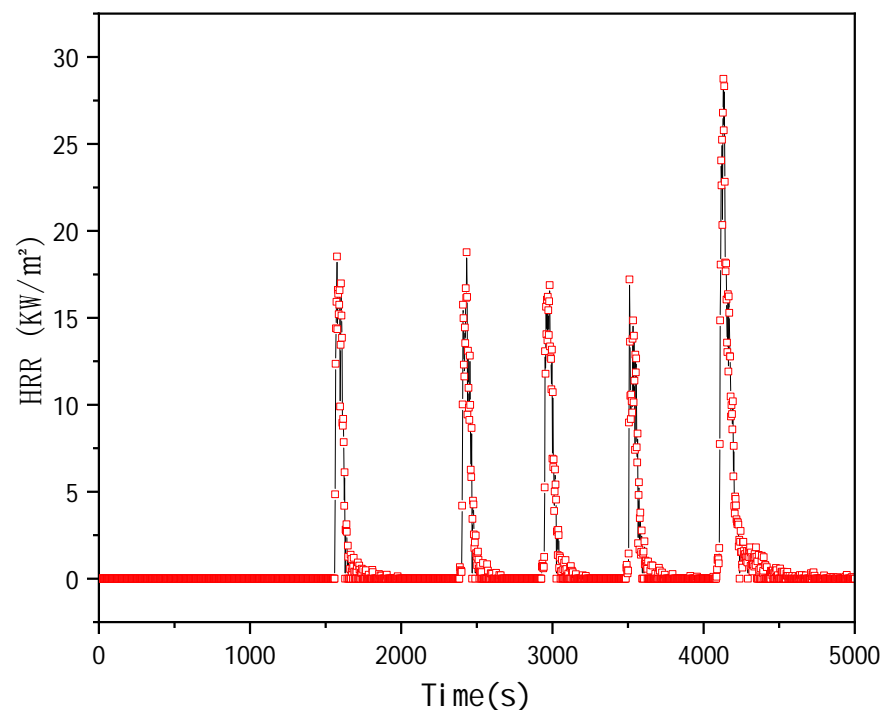


**Figure 9.** Heat release rate (HRR) of the LIBs as a function of time during the TR process.

As shown in Table 2, the knee points of the gas concentrations and HRR peaks occurred at 1563 s, 2403 s, 2949 s, 3387 s, and 4107 s. These values were earlier than the temperature parameter values (1591 s, 2453 s, 2966 s, 3552 s, and 4137 s) by 28 s, 50 s, 17 s, 165 s, and 30 s, respectively. They were earlier than the voltage parameter values (1585 s, 2430 s, 2945 s,

3500 s, and 4115 s) by 22 s, 27 s, −4 s, 113 s, and 8 s, respectively. However, these values were later than the mass parameter values (1445 s, 2290 s, 2840 s, 3400 s, and 3985 s) by 78 s, 113 s, 109 s, 13 s, and 122 s, respectively. Therefore, utilizing the module mass or gas concentration parameters provides similar warnings, on average, about 2 min earlier than the other parameters considered.

**Table 2.** The peak time and corresponding temperature of battery cells.

| Parameters  | The Knee Points (S) |      |      |      |      |
|-------------|---------------------|------|------|------|------|
|             | 1591                | 2453 | 2966 | 3552 | 4137 |
| Temperature | 1591                | 2453 | 2966 | 3552 | 4137 |
| Voltage     | 1585                | 2430 | 2945 | 3500 | 4115 |
| Mass        | 1445                | 2290 | 2840 | 3400 | 3985 |
| Gas         | 1563                | 2403 | 2949 | 3387 | 4107 |

## 10. Conclusions

The present study addresses the current limitations in meeting safety regulations for lithium-ion battery (LIB) modules in electric vehicles during thermal runaway (TR) events. It evaluates the cascading thermal failure characteristics of six-cell LIB modules in an experimental combustion chamber under an air environment. Various characteristic parameters, including LIB temperature, module voltage, module mass, and concentrations of venting gases in the combustion chamber, are analyzed in detail. The primary results can be summarized as follows:

1. The TR propagation process in the module shows sequential gas ejection and smoke combustion events for LIBs 1–4, followed by nearly simultaneous thermal failure of LIBs 5 and 6.
2. During each gas ejection event, the LIB temperatures reach peak values, the module mass and voltage exhibit step-wise decreases, and the concentrations of CO<sub>2</sub> and CO by volume increase, while the O<sub>2</sub> concentration decreases. These parameter changes provide distinct indications of TR events in individual LIBs of the module.
3. The order of warning effectiveness, from latest to earliest, is as follows: LIB temperature > module voltage > gas concentration > module mass. Compared to warnings based on LIB temperature alone, measurements of module mass and gas concentrations in the combustion chamber enable earlier warnings of thermal failure, on average, by approximately 2 min.

This work provides valuable insights for enhancing the safety and reliability of LIBs, improving fault detection systems, and extending the safe escape time beyond the requirements of Global Technical Regulation No. 20.

**Author Contributions:** Conceptualization, Y.W.; methodology, Y.W.; H.L. performed the data analysis; H.L. perform the original draft writing; Q.G. and Y.W. perform article review, commentary and revision; Y.W. acquisition of the financial support. All authors have read and agreed to the published version of the manuscript.

**Funding:** This research is generously supported by the National Natural Science Foundation of China (Youth Program Grant No. 52207240), Shandong Province Science and Technology Foundation (Youth Program Grant No. ZR2022QE099). The authors gratefully acknowledge the financial support from the Joint Science Foundation of Guangdong Province (Grant No. 21201910260000023) and Open-end Funds from State key Laboratory of automobile safety and energy conservation, from Tsinghua University (Grant No. KFY2221).

**Conflicts of Interest:** The authors declare no conflict of interest.

## References

1. Börger, A.; Mertens, J.; Wenzl, H. Thermal runaway and thermal runaway propagation in batteries: What do we talk about? *J. Energy Storage* **2019**, *24*, 100649. [[CrossRef](#)]
2. Feng, X.; Ouyang, M.; Liu, X.; Lu, L.; Xia, Y.; He, X. Thermal runaway mechanism of lithium ion battery for electric vehicles: A review. *Energy Storage Mater.* **2018**, *10*, 246–267. [[CrossRef](#)]
3. Chen, S.; Wang, Z.; Wang, J.; Tong, X.; Yan, W. Lower explosion limit of the vented gases from Li-ion batteries thermal runaway in high temperature condition. *J. Loss Prev. Process Ind.* **2020**, *63*, 103992. [[CrossRef](#)]
4. Abd-El-Latif, A.A.; Sichler, P.; Kasper, M.; Waldmann, T.; Wohlfahrt-Mehrens, M. Insights Into Thermal Runaway of Li-Ion Cells by Accelerating Rate Calorimetry Coupled with External Sensors and Online Gas Analysis. *Batter. Supercaps* **2021**, *4*, 1135–1144. [[CrossRef](#)]
5. Zhu, M.H.; Yao, J.J.; Qian, F.Y.; Luo, W.Y.; Chen, Y.; Zhao, L.Y.; Chen, M.Y. Study on Thermal Runaway Propagation Characteristics of Lithium Iron Phosphate Battery Pack under Different SOCs. *Electronics* **2023**, *12*, 200. [[CrossRef](#)]
6. Ma, B.; Liu, J.; Yu, R. Study on the Flammability Limits of Lithium-Ion Battery Vent Gas under Different Initial Conditions. *ACS Omega* **2020**, *5*, 28096–28107. [[CrossRef](#)] [[PubMed](#)]
7. Chen, S.; Gao, Z.; Sun, T. Safety challenges and safety measures of Li-ion batteries. *Energy Sci. Eng.* **2021**, *9*, 1647–1672. [[CrossRef](#)]
8. Wang, Z.; Zhu, K.; Hu, J.; Wang, J. Study on the fire risk associated with a failure of large-scale commercial LiFePO<sub>4</sub>/graphite and LiNi<sub>x</sub>CoyMn<sub>1-x-y</sub>O<sub>2</sub>/graphite batteries. *Energy Sci. Eng.* **2019**, *7*, 411–419. [[CrossRef](#)]
9. Jin, C.; Sun, Y.; Wang, H.; Lai, X.; Wang, S.; Chen, S.; Rui, X.; Zheng, Y.; Feng, X.; Wang, H.; et al. Model and experiments to investigate thermal runaway characterization of lithium-ion batteries induced by external heating method. *J. Power Sources* **2021**, *504*, 230065. [[CrossRef](#)]
10. Chong, D.; Zhu, M.; Zhao, Q.; Chen, W.; Yan, J. A Review on Thermal Design of Liquid Droplet Radiator System. *J. Therm. Sci.* **2021**, *30*, 394–417. [[CrossRef](#)]
11. Ouyang, D.X.; Chen, M.Y.; Huang, Q.; Weng, J.W.; Wang, Z.; Wang, J. A Review on the Thermal Hazards of the Lithium-Ion Battery and the Corresponding Countermeasures. *Appl. Sci.* **2019**, *9*, 2483. [[CrossRef](#)]
12. Fernandes, Y.; Bry, A.; de Persis, S. Identification and quantification of gases emitted during abuse tests by overcharge of a commercial Li-ion battery. *J. Power Sources* **2018**, *389*, 106–119. [[CrossRef](#)]
13. Zheng, S.; Wang, L.; Feng, X.; He, X. Probing the heat sources during thermal runaway process by thermal analysis of different battery chemistries. *J. Power Sources* **2018**, *378*, 527–536. [[CrossRef](#)]
14. Kong, D.; Wang, G.; Ping, P.; Wen, J. Numerical investigation of thermal runaway behavior of lithium-ion batteries with different battery materials and heating conditions. *Appl. Therm. Eng.* **2021**, *189*, 116661. [[CrossRef](#)]
15. Lopez, C.F.; Jeevarajan, J.A.; Mukherjee, P.P. Experimental Analysis of Thermal Runaway and Propagation in Lithium-Ion Battery Modules. *J. Electrochem. Soc.* **2015**, *162*, A1905–A1915. [[CrossRef](#)]
16. Zhou, Z.; Zhou, X.; Wang, D.; Li, M.; Wang, B.; Yang, L.; Cao, B. Experimental analysis of lengthwise/transversal thermal characteristics and jet flow of large-format prismatic lithium-ion battery. *Appl. Therm. Eng.* **2021**, *195*, 117244. [[CrossRef](#)]
17. Ren, D.; Hsu, H.; Li, R.; Feng, X.; Guo, D.; Han, X.; Lu, L.; He, X.; Gao, S.; Hou, J.; et al. A comparative investigation of aging effects on thermal runaway behavior of lithium-ion batteries. *eTransportation* **2019**, *2*, 100034. [[CrossRef](#)]
18. Weng, J.W.; Xiao, C.R.; Ouyang, D.X.; Yang, X.Q.; Chen, M.Y.; Zhang, G.Q.; Yuen, R.K.K.; Wang, J. Mitigation effects on thermal runaway propagation of structure-enhanced phase change material modules with flame retardant additives. *Energy* **2022**, *239*, 122087. [[CrossRef](#)]
19. Li, Y.; Qi, F.; Guo, H.; Guo, Z.P.; Xu, G.; Liu, J. Numerical investigation of thermal runaway propagation in a Li-ion battery module using the heat pipe cooling system. *Numer. Heat Transf. Part A-Appl.* **2019**, *75*, 183–199. [[CrossRef](#)]
20. Huang, Y.; Wu, Y.; Liu, B. Experimental investigation into the use of emergency spray on suppression of battery thermal runaway. *J. Energy Storage* **2021**, *38*, 102546. [[CrossRef](#)]
21. Wang, Z.; Wang, J. An experimental investigation of the degradation and combustion behaviors associated with lithium ion batteries after different aging treatments. *J. Clean. Prod.* **2020**, *272*, 122708. [[CrossRef](#)]
22. Hao, W.; Yuan, Z.; Li, D.; Zhu, Z.; Jiang, S. Study on mechanical properties and failure mechanism of 18650 Lithium-ion battery using digital image correlation and acoustic emission. *J. Energy Storage* **2021**, *41*, 102894. [[CrossRef](#)]
23. Zhao, J.; Lu, S.; Fu, Y.; Ma, W.; Cheng, Y.; Zhang, H. Experimental study on thermal runaway behaviors of 18650 li-ion battery under enclosed and ventilated conditions. *Fire Saf. J.* **2021**, *125*, 103417. [[CrossRef](#)]
24. Ostanek, J.K.; Li, W.; Mukherjee, P.P.; Crompton, K.R.; Hacker, C. Simulating onset and evolution of thermal runaway in Li-ion cells using a coupled thermal and venting model. *Appl. Energy* **2020**, *268*, 114972. [[CrossRef](#)]
25. Wang, Q.; Mao, B.; Stolarov, S.I.; Sun, J. A review of lithium ion battery failure mechanisms and fire prevention strategies. *Prog. Energy Combust. Sci.* **2019**, *73*, 95–131. [[CrossRef](#)]
26. Weng, J.W.; Ouyang, D.X.; Liu, Y.H.; Chen, M.Y.; Li, Y.P.; Huang, X.Y.; Wang, J. Alleviation on battery thermal runaway propagation: Effects of oxygen level and dilution gas. *J. Power Sources* **2021**, *509*, 230340. [[CrossRef](#)]
27. Feng, X.; Sun, J.; Ouyang, M.; Wang, F.; He, X.; Lu, L.; Peng, H. Characterization of penetration induced thermal runaway propagation process within a large format lithium ion battery module. *J. Power Sources* **2015**, *275*, 261–273. [[CrossRef](#)]



28. Huang, P.; Ping, P.; Li, K.; Chen, H.; Wang, Q.; Wen, J.; Sun, J. Experimental and modeling analysis of thermal runaway propagation over the large format energy storage battery module with Li<sub>4</sub>Ti<sub>5</sub>O<sub>12</sub> anode. *Appl. Energy* **2016**, *183*, 659–673. [[CrossRef](#)]
29. Liu, X.; Wu, Z.B.; Stoliarov, S.I.; Denlinger, M.; Masias, A.; Snyder, K. A Thermo-Kinetic Model of Thermally-Induced Failure of a Lithium Ion Battery: Development, Validation and Application. *J. Electrochem. Soc.* **2018**, *165*, A2909–A2918. [[CrossRef](#)]
30. Mishra, D.; Shah, K.; Jain, A. Investigation of the Impact of Flow of Vented Gas on Propagation of Thermal Runaway in a Li-Ion Battery Pack. *J. Electrochem. Soc.* **2021**, *168*, 060555. [[CrossRef](#)]
31. Kim, J.; Mallarapu, A.; Finegan, D.P.; Santhanagopalan, S. Modeling cell venting and gas-phase reactions in 18650 lithium ion batteries during thermal runaway. *J. Power Sources* **2021**, *489*, 229496. [[CrossRef](#)]
32. Mao, B.; Zhao, C.; Chen, H.; Wang, Q.; Sun, J. Experimental and modeling analysis of jet flow and fire dynamics of 18650-type lithium-ion battery. *Appl. Energy* **2021**, *281*, 116054. [[CrossRef](#)]
33. Cai, T.; Valecha, P.; Tran, V.; Engle, B.; Stefanopoulou, A.; Siegel, J. Detection of Li-ion battery failure and venting with Carbon Dioxide sensors. *eTransportation* **2021**, *7*, 100100. [[CrossRef](#)]
34. GB/T20284-2006; Single Burning Item Test for Building Materials and Products. Fire Research Institute: Sichuan, China, 2006. (In Chinese)
35. Röder, P.; Baba, N.; Wiemhöfer, H.D. A detailed thermal study of a Li[Ni<sub>0.33</sub>Co<sub>0.33</sub>Mn<sub>0.33</sub>]O<sub>2</sub>/LiMn<sub>2</sub>O<sub>4</sub>-based lithium ion cell by accelerating rate and differential scanning calorimetry. *J. Power Sources* **2014**, *248*, 978–987. [[CrossRef](#)]

**Disclaimer/Publisher’s Note:** The statements, opinions and data contained in all publications are solely those of the individual author(s) and contributor(s) and not of MDPI and/or the editor(s). MDPI and/or the editor(s) disclaim responsibility for any injury to people or property resulting from any ideas, methods, instructions or products referred to in the content.